Marine Research
of the National Academy of Marine Research
ISSN: 2709-6629 (Vol.1 Iss.1)
GPN: 2011200033

DOI: http://dx.doi.org/10.29677/MR.202112_1(1).0002
2021, 1(1), 24-35

The Design and Analysis of the Wells Turbine in an Oscillating Water Column Wave Power System

Ching-Yeh Hsin* Jia-Yang Lai Yang-Cheng Chiu

Department of Systems Engineering and Naval Architecture,
National Taiwan Ocean University

ABSTRACT

Wave energy is a type of marine renewable energy, and an Oscillating Water Column wave power system (OWC) is a converter with higher efficiency. The turbine in the system determines the efficiency of energy conversion and directly affects the performance of wave power generation. This paper presents the study conducted on the widely-used Wells turbine in an oscillating water column wave power system and the blade design method with evaluations and performance comparison of designs. In this paper, different designs were carried out by both potential flow and viscous flow methods, and the performance of each was confirmed and compared. It has been found that the design with a camber distribution is better than the reference geometry without a camber distribution. The average torque and efficiency are close to the reference geometry, but the stall is delayed. Next, the blades designed with an optimized skew distribution have achieved better performance than zero-skew distribution. The mean torque coefficient is increased from 0.057 to 0.125, and the mean efficiency coefficient is increased from 0.452 to 0.483 with the designed skew distribution. Finally, a comparison between single-stage and contra-rotating turbines has been conducted, and although contra-rotating turbines generate greater torque, they have lower efficiency.

Keywords: wave energy, Oscillating Water Column, Wells turbine, blade design, CFD.

* Corresponding author, E mail: hsin@mail.ntou.edu.tw

Received 9 August 2021, Accepted 30 September 2021.

1 INTRODUCTION

This paper will discuss and evaluate the Wells turbine in an Oscillating Water Column (OWC) wave power system and develop blade design methods. Wave energy is a type of marine renewable energy; since Taiwan is surrounded by oceans, wave energy is a natural resource stored around us. According to the research by the Industrial Technology Research Institute (Hsu and Yen, 2007), if wave energy reaches 10 kW/m, it has development value. The wave energy team of the National Taiwan Ocean University conducted a wave energy survey in northeastern Taiwan (Tzang et al., 2011), which shows that each winter, between November and February, the wave energy can reach above 10 kW/m about 30 – 70% of the time in Keelung Port and Longdong.

There are indeed many types of ocean wave energy conversion systems (WEC). While each one has progressed in terms of research and development, OWC is at the leading edge among various WEC. The operating principle of the OWC is that the surface of the seawater in a chamber rises or falls due to waves; the air is discharged or sucked in from the tunnel, this airflow drives the turbine in the tunnel, and finally, the turbine generator generates electricity.

The pioneers of OWC operation in the real sea are the well-known Pico and LIMPET (Land Installed Marine Power Energy Transmitter). LIMPET (Boake et al., 2002) started the construction of OWC on the Isle of Islay in the west of Scotland in 1998. It was completed in 2000 and underwent efficacy tests during the whole year. The original estimate for the average annual power generation efficiency of the LIMPET prototype machine was 40%, but after a year of testing, it is found that the annual average power generation efficiency was only about 22%. Although the efficiency of LIMPET did not reach the original estimate, it was in operation for more than 10 years, showing its long-term durability. In the OWC system, the key conversion element is the turbine. One of the features of OWC is that the airflow flows in both directions, which, therefore, the design of the turbine blade must consider. In this regard, the two most frequently used turbines in OWC are the Wells turbine and the impulse turbine. This paper will focus on the Wells turbine (Raghunathan et al., 1982; Raghunathan, 1995; Shehata et al., 2017; Starzmann and Carolus, 2014). The Wells turbine is an axial-flow horizontal turbine. Its blades are usually symmetrical, so that the flow in both directions can drive the turbine to rotate, and its rotation uses the tangential component of the airfoil lift to generate torque.

2 GEOMETRY AND METHOD USED IN THE DESIGN

2.1 Design Method

The numerical methods used in our design procedure includes both the potential flow and the viscous flow RANS methods. We have developed a potential flow boundary element method for the Wells turbine blade design. The computations of the viscous flow RANS method are carried out by commercial CFD software STAR-CCM+. The design procedure is to first apply the computationally efficient potential flow method for design, and then use the viscous flow tool to confirm the design. For the geometric designs, we hope to explore as many possibilities as we can; therefore, the computationally efficient potential flow method is used. On the other hand, the viscous flow method is closer to real physics, and it can confirm the performance of the designed geometry. The presented method takes into account both the efficiency of designs and the accuracy of the physical characteristics.

Marine Research of the National Academy of Marine Research
DOI: 10.29677/MR.202112_1(1).0002

2.2 Geometry for the Design

We use the geometry in (Halder et al., 2017) as the designed geometry, and the experimental data of the same geometry in (Curran and Gato, 1997) is used for validations of computational results. Figure 1 shows the reference geometry used for the design; we refer to it as "prototype" in this paper. Table 1 also shows the basic geometric parameters of the Wells turbine for design.

Table 1. The basic geometric parameters of the Wells turbine for design.

Parameter	Dimension
Blade profile	NACA0015
Chord length, C	0.125 m
Number of blades	8
Blade maximum thickness	15% of C
Solidity at mean radius	0.644
Casing radius	0.3 m
Hub radius	0.2 m
Tip clearance (TC)	1% of C
Turbine rotational speed	2,000rpm

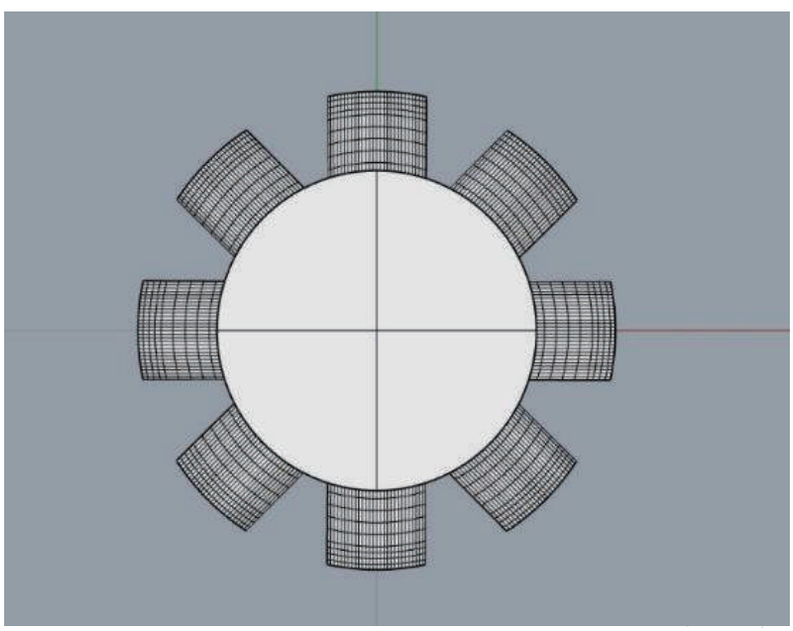

Figure 1. The reference geometry for design; we refer to it as "prototype" in this paper.

Marine Research of the National Academy of Marine Research
DOI: 10.29677/MR.202112_1(1).0002

3 COMPUTATIONAL RESULTS AND ANALYSIS

3.1 Accuracy of the Computational Method

The commercial CFD software STAR-CCM+ based on the finite volume method is used in this research. The SST k-ω turbulence model is used, and the grid arrangement is shown in Figure 2. Definitions of the dimensionless parameters in the calculation are explained in Equation 1. Next, the computational results obtained by the viscous flow and potential flow methods are respectively demonstrated, and results of the "prototype" geometry (Halder et al., 2017) are verified by experimental values and computational results in the literature.

$$\begin{aligned}
&\text{Flow coefficient: } \mathrm{U}^* = \frac{V}{\omega R};\ V:\text{Flow speed}\\
&\text{Torque coefficient: } T^* = \frac{T}{\rho\omega^3 R^5};\ T:\text{Torque}\\
&\text{Pressure drop coefficient: } \Delta P^* = \frac{\Delta P}{\rho\omega^2 R^2};\ \Delta P:\text{Pressure drop}\\
&\text{Efficiency coefficient: } \eta^* = \frac{T\omega}{Q\Delta P};\ Q:\text{Volume flow rate;}\\
&\mathrm{R}:\text{Rotor radius;}\qquad \omega:\text{Rotational speed}
\end{aligned} \tag{1}$$

Figure 3 shows the comparison between the calculated value of the pressure drop coefficient and the experimental value. The thick black dotted line in the figure is the experimental value, the black thin dotted line represents the computational results from the literature, and the black square marks the result of our calculation. The comparison in the figure shows that the result of our computation is slightly underestimated, but the basic trend is considered to be consistent. For the torque coefficient, the computational result is very close to the experimental data and the calculated value in the literature, with the exception of the vicinity of $U^*=0.2125$. The efficiency coefficient is calculated from the pressure drop and the torque coefficient; therefore, the comparison among the computational results of ours, from the literature, and the experimental data are all close. The results show that our viscous flow computation is credible. We then continue to investigate the computational results of the potential flow boundary element method (BEM). Figure 4 shows the comparison among the calculated value of the pressure drop coefficient, the torque coefficient and the efficiency coefficient by BEM, and the experimental data. It can be seen that the calculated value by BEM is quite close to the experimental value. From the calculation results in this section, it can be concluded that both the potential flow and viscous flow computational methods are credible.

DOI: 10.29677/MR.202112_1(1).0002

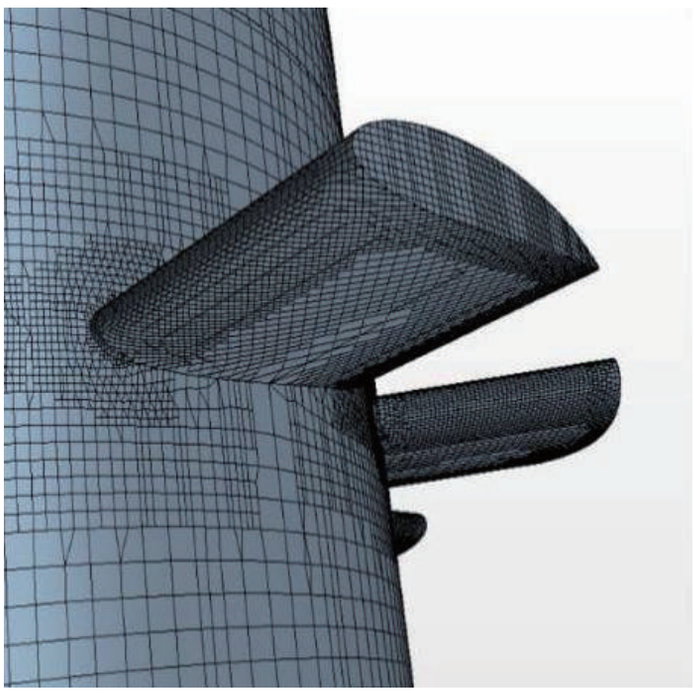

Figure 2. The grid arrangement of the CFD computations.

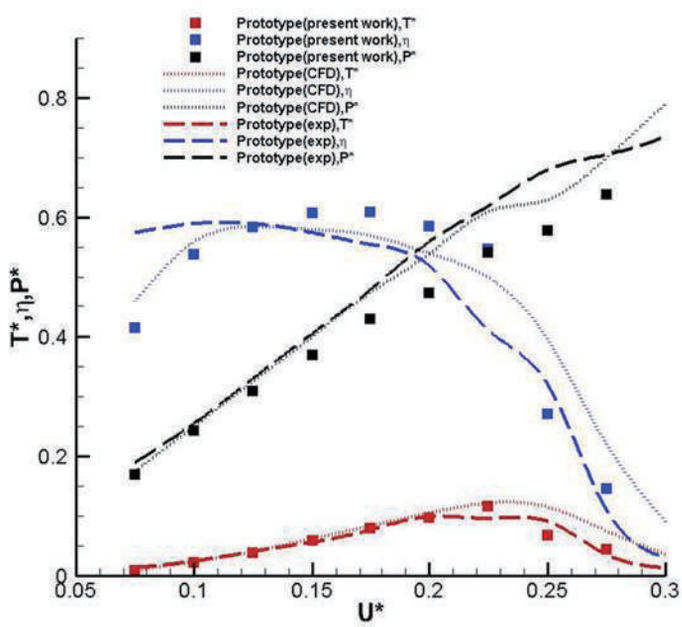

Figure 3. Comparison of pressure drop, torque, and efficiency coefficients from the presented computational results, calculated values from the literature, and experimental data.

DOI: 10.29677/MR.202112_1(1).0002

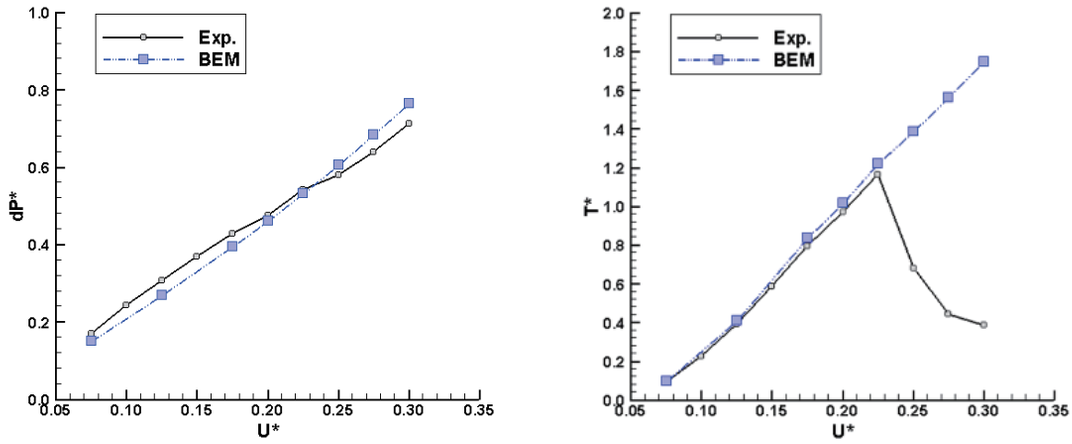

Figure 4. The pressure drop coefficient (left) and torsion coefficient (right) calculated by the potential flow boundary element method are compared with the experimental data.

3.2 Design Procedure

We have confirmed the credibility of computational tools; we then used these computational tools to design the Wells turbine blade geometry. Since the inflow of the Wells turbine is a repetitive two-directional flow, unless the blades can rotate, the pitch angle becomes an unnecessary design parameter. In this paper, the designs of skew and camber distributions are demonstrated. The design procedure is as follows:

1. The blade thickness is mainly based on the consideration of structural strength. We decided to adopt NACA0015 section; its thickness is 15% of chord length.

2. The camber distribution is preliminarily designed by the potential flow BEM method, and the design is then confirmed with the viscous flow method.

3. Since the skew distribution is referred from (Halder et al., 2017), the viscous flow method is directly adopted for the design of skew distribution.

The design model geometry is shown in Table 1, the design speed is 15.56 m/s, and the model design power is 3.3kW.

3.3 Skew Distribution

The geometry shown in the literature (Halder et al., 2017) is used as the reference geometry ("prototype" geometry). For the design of skew distribution, the distribution presented in (Halder et al., 2017) has been varied, and the performance of each is compared to that in (Halder et al., 2017). It is found that the distribution that shows the best performance is still the one designed by (Halder et al., 2017). This skew distribution is called "optimization" geometry, and it is used to demonstrate the advantages of the skew. Figure 5 shows the performance difference between the "prototype" geometry (without skew) and the "optimization" geometry. The solid line is from "prototype" geometry, and the dashed line is from "optimization" geometry. The red lines are pressure drop coefficients, the black lines are torque coefficients, and the blue lines are efficiency coefficients. The difference in performance between two geometries are:

Marine Research of the National Academy of Marine Research
DOI: 10.29677/MR.202112_1(1).0002

1. The geometry with skew ("optimization") gives lower pressure drop.

2. In terms of torque, the geometry with skew ("optimization") is slightly lower than the "prototype" geometry at low speeds. However, the "prototype" geometry has a stall at higher speeds, and the torque drops off quickly. The "optimization" geometry proves to have a better performance due to the skew distribution.

3. Due to the drop of torque, the efficiency of "prototype" geometry also drops off quickly at higher speeds. On the other hand, the "optimization" geometry achieves stable efficiency at higher speeds and maintains a wider speed range. That means, the geometry with a good skew distribution can provide a wider operating range.

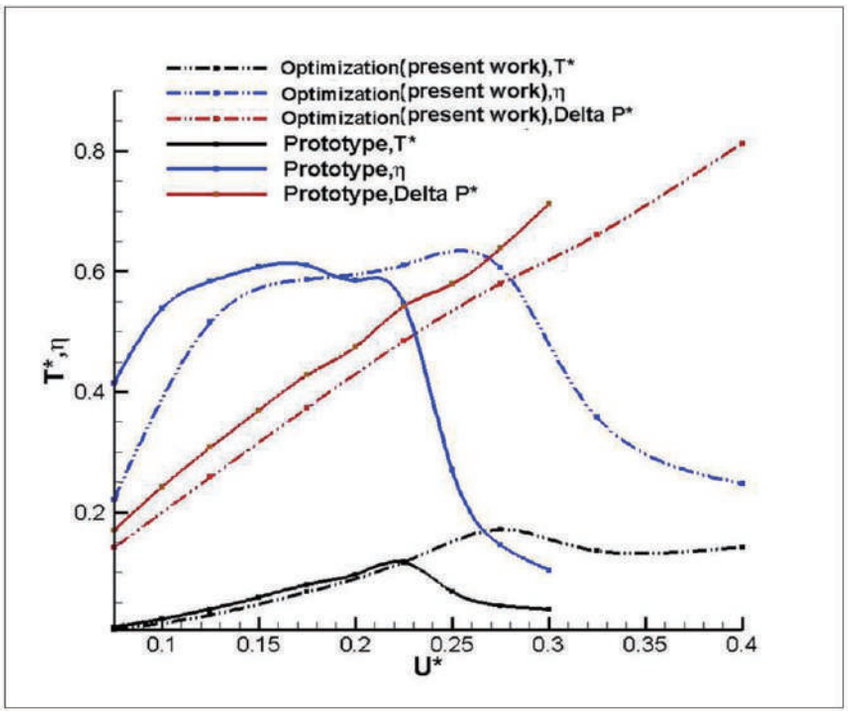

Figure 5. The performance difference between "prototype" geometry and "optimization" geometry, where the solid line is from "prototype" geometry, and the dashed line is from "optimization" geometry. The red lines are pressure drop coefficients, the black lines are torque coefficients, and the blue lines are efficiency coefficients.

3.4 Camber Distribution

The camber distribution is designed by the potential flow BEM, and the viscous flow calculation is then used to confirm the design. The inflow of a Wells turbine is two-directional. In Figure 6, "$a = 0.8(-x)$" means the inflow from the suction side, and "$a = 0.8(+x)$" means the inflow from the pressure side. Figure 6 shows the comparison of torque and efficiency coefficients between the geometries with and without the camber distribution. It can be seen that compared to the geometry without a camber, the performance of "$a = 0.8(-x)$" (inflow from suction side) is better, and "$a = 0.8(+x)$" is worse. The average performance is about the same. However, the stall is delayed. The camber distribution of $a = 0.8$ meanline provides a better performance overall.

Marine Research of the National Academy of Marine Research
DOI: 10.29677/MR.202112_1(1).0002

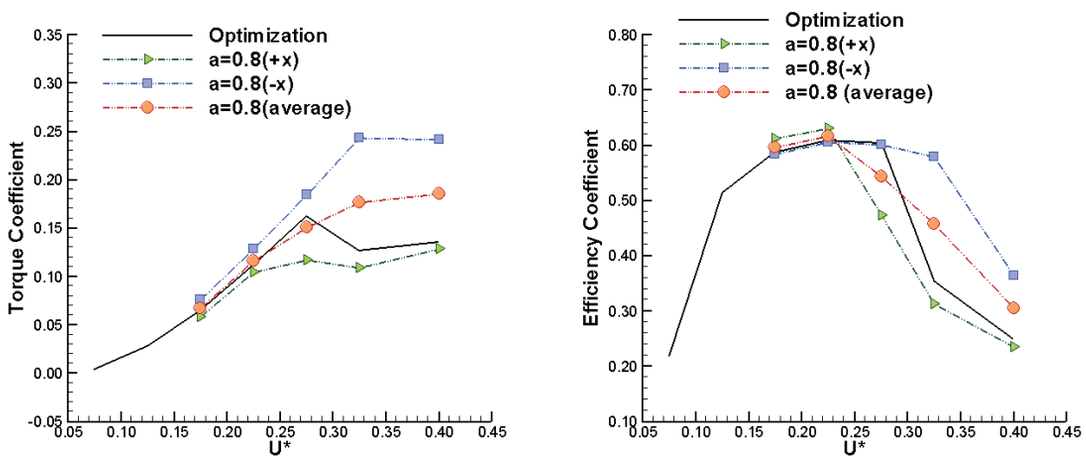

Figure 6. The torque coefficient (left) and efficiency coefficient (right) of the inflow in two directions and their average values for a = 0.8 meanline design. "a = 0.8(-x)" means inflow from the suction side, and "a = 0.8(+x)" means inflow from the pressure side.

3.5 Performance Comparison of "Prototype" and Designed Geometries

The design having been completed, the results of different design parameters are summarized in Table 2. For different design parameters, the torque and the efficiency coefficients of the prototype and the designed geometry are compared to each other. The comparisons of both the maximum and mean values are summarized in Table. 2.

Table 2. Performance Comparison of "Prototype" and Designed Geometries.

			" Prototype" Geometry	Designed Geometry
Operating Range			U^* = 0.075-0.300	U^* = 0.175-0.400
Skew	Torque	Max.	At U^* = 0.225, the torque coefficient is 0.116.	At U^* = 0.275, the torque coefficient is 0.168.
		Mean	0.057	0.125
	Efficiency	Max.	At U^* = 0.175, the efficiency coefficient is 0.610.	At U^* = 0.225, the efficiency coefficient is 0.612.
		Mean	0.452	0.483
Camber	Torque	Max.	At U^* = 0.225, the torque coefficient is 0.116.	At U^* = 0.400, the torque coefficient is 0.185.
		Mean	0.057	0.139
	Efficiency	Max.	At U^* = 0.175, the efficiency coefficient is 0.610.	At U^* = 0.225, the efficiency coefficient is 0.619.
		Mean	0.452	0.500

Marine Research of the National Academy of Marine Research
DOI: 10.29677/MR.202112_1(1).0002

4 PERFORMANCE COMPARISON WITH A CONTRA-ROTATING WELLS TURBINE

A single-stage turbine is our design goal, yet we discuss the performance of multi-stage Wells turbines by computation. The multi-stage Wells turbine used is a contra-rotating Wells turbine, which was the type used in LIMPET. The geometry of the contra-rotating turbine presented in this paper is shown in Figure 7, and the distance between two stages is one chord length (0.125m). Figure 8 shows the comparison between torques of the contra-rotating and the single stage turbines ("Optimization"). It shows that the torque of the upstream stage of contra-rotation is larger than that of the single stage, while that of the downstream stage is smaller than that of the single stage. We also show the comparison of the total torque of the contra-rotating turbine and that of the single stage; the torque of the contra-rotating turbine is almost twice that of the single stage turbine. Figure 9 shows a comparison of the efficiency of contra-rotating turbine with that of the single stage; the efficiency of the contra-rotating turbine is lower than that of the single stage turbine.

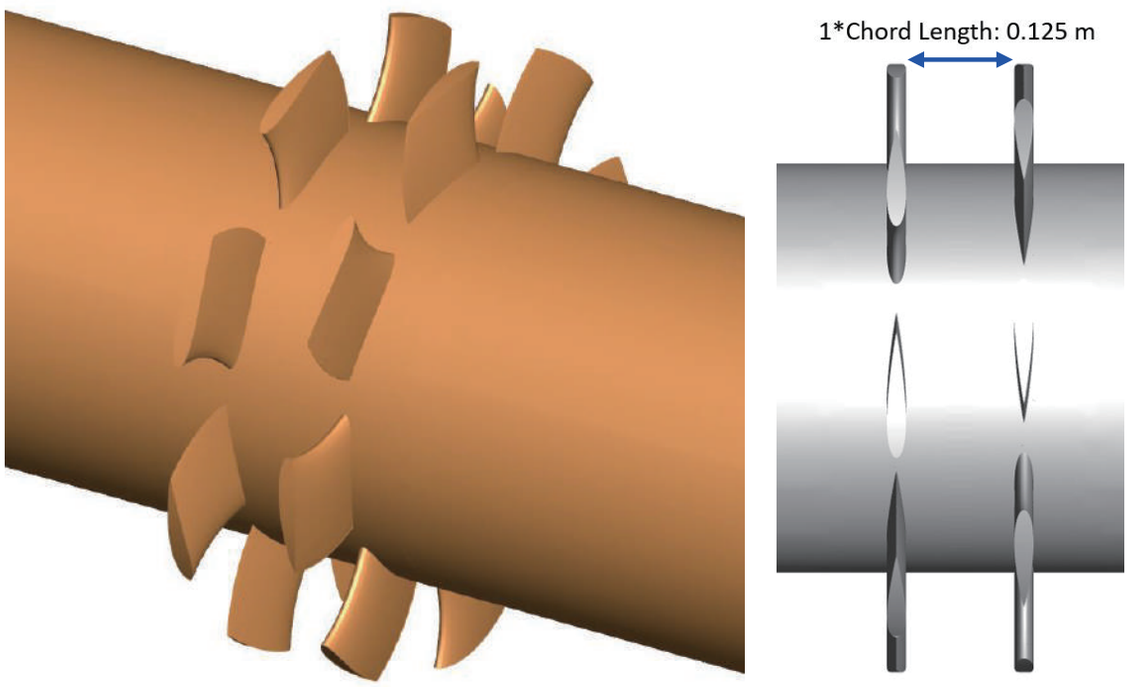

Figure 7. The geometry of the contra-rotating turbine presented in this paper (left). The distance between the two stages (right) is one chord length (0.125m).

Marine Research of the National Academy of Marine Research
DOI: 10.29677/MR.202112_1(1).0002

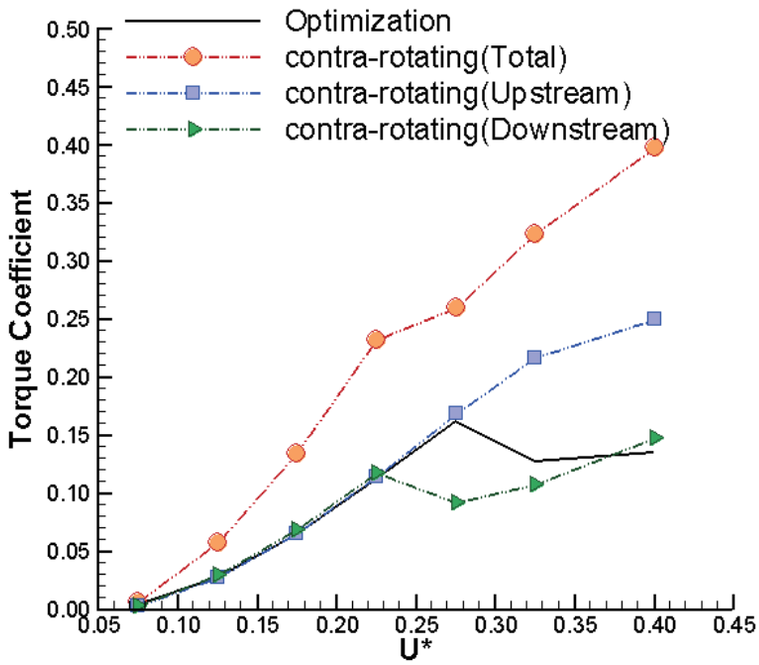

Figure 8. A comparison of torques (upstream stage, downstream stage and total) of the contra-rotating and the single stage turbines ("Optimization").

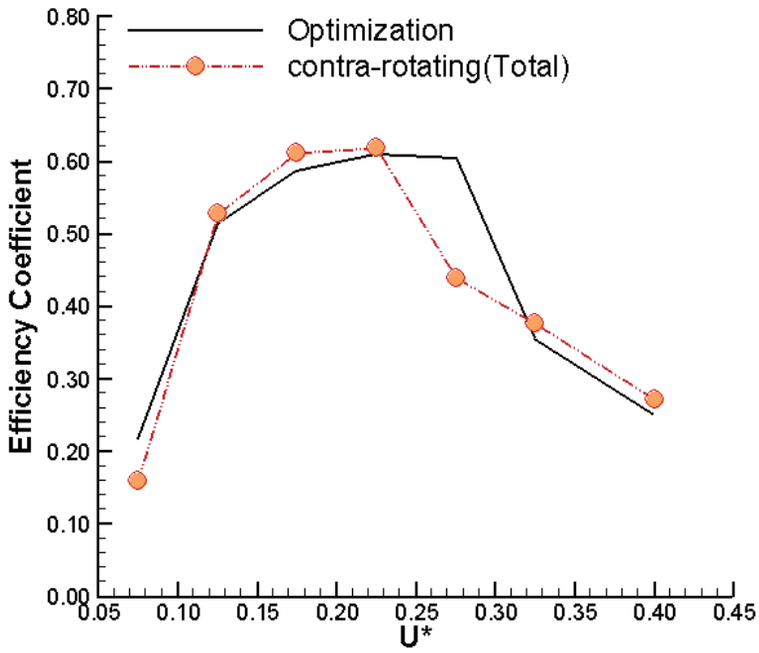

Figure 9. A comparison of the efficiency coefficients of the contra-rotating and the single stage turbines ("Optimization").

Marine Research of the National Academy of Marine Research
DOI: 10.29677/MR.202112_1(1).0002

5 CONCLUSIONS

In this paper, we have demonstrated a design procedure for the Wells turbine, and both the potential flow and viscous flow methods are used for the purpose of design efficiency. The performances of designed camber and skew distributions are shown. We conclude that:

1. The a = 0.8 meanline camber distribution is adopted in the design. It is found that the geometry with camber has almost the same average torque and efficiency as the reference geometry, but the stall is delayed, and operating range is increased.

2. The stall happens at a higher speed for the geometry with skew, and it thus provides a stable efficiency and a wider operating range.

3. After completing the design, we have also calculated the performance of a contra-rotating Wells turbine, and compared it with the single-stage turbine. Although contra-rotating turbines generate greater torque, they have lower efficiency.

ACKNOWLEDGEMENTS

This research is in part a result of the "Preliminary Study on Turbine Design of Oscillating Water Column Wave Power System" funded by the National Academy of Marine Research. The authors would like to express their appreciation for their financial support and technical guidance.

NOMENCLATURE

ΔP	The pressure drop between inlet and outlet of OWC turbine
T	Torque of the turbine blade
V	Flow speed
ω	Rotational speed
Q	Volume flow rate
R	Rotor radius
$\mathrm{U}^* = V / \omega R$	Flow coefficient
$T^* = \frac{T}{\rho \omega^3 R^5}$	Torque coefficient
$\Delta P^* = \frac{\Delta P}{\rho \omega^2 R^2}$	Pressure drop coefficient
$\eta^* = \frac{T\omega}{Q\Delta P}$	Efficiency coefficient

DOI: 10.29677/MR.202112_1(1).0002

REFERENCES

Boake, C. B., Whittaker, T. J. T., Folley, M., & Ellen, H. (2002). Overview and Initial Operational Experience of the LIMPET Wave Energy Plant. *Proceedings of the 12th International Offshore and Polar Engineering Conference, Kitakyushu, Japan,* 586-594.

Curran, R., & Gato, L. M. C. (1997). The energy conversion performance of several types of Wells turbine designs. *Proceedings of the Institution of Machanical Engineers, Part A: Journal of Power and Energy, 211*(2), 133-145. https://doi.org/10.1243%2F0957650971537051

Halder, P., Rhee, S.H., & Samad, A. (2017). Numerical optimization of Wells turbine for wave energy extraction. *International Journal of Naval Architecture and Ocean Engineering, 9*(1), 11-24. https://doi.org/10.1016/j.ijnaoe.2016.06.008

Hsu, B. H., & Yen, C. W. (2007). Introduction to the Development Prospects of Ocean Energy in Taiwan. *Physics Bimonthly, 29*(3), 718-726. (in Chinese)

Raghunathan, S., Tan, C.P., & Wells, N. A. J. (1982). Theory and performance of a Wells turbine. *Journal of Energy, 6*(2), 157-160. https://doi.org/10.2514/3.48047

Raghunathan, S. (1995). The wells air turbine for wave energy conversion. *Progress in Aerospace Sciences, 31*(4), 335-386. https://doi.org/10.1016/0376-0421(95)00001-F

Shehata, A. S., Xiao, Q., Saqr, K. M., & Alexander, D. (2017). Wells turbine for wave energy conversion: a review. *International Journal of Energy Research, 41*(1), 6-38. https://doi.org/10.1002/er.3583

Starzmann, R., & Carolus, T. (2014). Effect of Blade Skew Strategies on the Operating Range and Aeroacoustic Performance of the Wells Turbine. *Journal of Turbomachinery, 136*(1), 011003. https://doi.org/10.1115/1.4025156

Tzang, S. Y., Chen, J. H., Yang, J. Z., & Wang, C. C. (2011). The analysis on wave power potentials on the northeast coastal waters of Taiwan . *Proceedings of the 11th International Conference on Fluid Control, Measurements and Visualization, Keelung, Taiwan.*

DOI: 10.29677/MR.202112_1(1).0002